Numerical and experimental investigation for the effect of permeability of spur dikes on local scour

Riham Mohsen Ezzeldin

ABSTRACT

The effect of using permeable spur dikes on the produced maximum scour depth compared to that of solid spur dikes is numerically investigated. The numerical model used for such purpose is the Nays-2DH model of the International River Interface Cooperative (iRIC) software package for bed and bank erosion. The model results are verified using the experimental data collected in this study by conducting experiments on five different models of spur dikes having different opening ratios. Using the statistical performance indices, the root mean square error and the coefficient of determination, the results showed an acceptable agreement between the numerical model results for the relative maximum scour depth defined by the ratio of the maximum scour depth to the flow depth and their corresponding observed values. A new empirical equation using nonlinear regression is developed using the experimental data collected in this study and tested with another existing empirical equation available in the literature for their accuracy in determining the relative maximum scour depth.

Key words | impermeable, Nays-2DH, permeable, scour depth, spur dikes

Riham Mohsen Ezzeldin
Irrigation and Hydraulics Department,
Faculty of Engineering,
Mansoura University,
Mansoura, DK,
Egypt
E-mail: *eng_ezzeldin@hotmail.com*

NOTATION

B	Channel bottom width
d_{50}	Mean sediment grain size
d_s	Maximum scour depth
d_{se}	Maximum scour depth, Equation (1)
F_r	Froude number
g	Gravitational acceleration
h	Water depth at time t
H	Total water depth
C_f	Drag coefficient of the bed shear stress
L	Spur dike length
n	Number of openings
n_m	Manning's coefficient of roughness
P_r	Opening ratio
q_{bx}	Bed load transport in x direction
q_{by}	*B*ed load transport in y direction
R	Opening ratio, Equation (1)
r_b	Hydraulic radius of bed
S_g	Grain specific weight
t	Time
u	Depth-averaged velocity in x direction
v	Depth-averaged velocity in y direction
V	Average approaching flow velocity
V_c	Critical velocity at incipient flow condition
x	Width of opening
y	Water depth
z	Bed elevation
ν_t	Eddy viscosity coefficient
λ	Porosity of the bed material
τ_x	Component of the shear stress of river bed in x direction
τ_y	Components of the shear stress of river bed in y direction

doi: 10.2166/hydro.2019.114

τ_* Non-dimensional bed shear stress
τ_{*c} Critical shear stress
Δt Time step

INTRODUCTION

Spur dikes are simple structures used to protect river banks from erosion by deviating the flow away from the banks towards the center of the river. However, their construction causes scour activities in their vicinity due to the formation of horseshoe, wake vortices and vertical component of down flow (Ettema & Muste 2004), and which may cause failure to the spur dike itself. Spur dikes can be permeable or impermeable. For permeable spur dikes, the flow partly penetrates the structure which results in a considerable reduction in velocity, vortex strength, and shear force at the nose of the spur dike (Li *et al.* 2005), and hence a remarkable reduction of maximum scour depth is observed (Fukuoka *et al.* 2000). As well, permeable spur dikes have the advantages of being more stable and requiring easier maintenance than impermeable ones (Kang *et al.* 2011). Scour around spur dikes occurs under clear water conditions where there is no transport of sediment by the approaching flow to the region of scour activities around the spur dike or under live bed scour where sediment is transported by the approaching flow as bed load or suspended load to the scour hole at the spur dike (Pandy *et al.* 2015).

Extensive numerical and experimental research has been conducted for predicting scour geometry around impermeable spur dikes while scour activities around permeable spur dikes have not attracted such concern. Recently, Gu *et al.* (2011) experimentally studied the influence of the aspect ratio defined by the interval between a series of permeable spur dikes to the length of the dikes on the transport of suspended sediment in open channels. Nasrollahi *et al.* (2008) experimentally investigated the local scour at permeable spur dikes under clear water scour condition. The flow intensity defined by the ratio of the average approaching flow velocity V to the critical velocity at incipient flow condition V_c was assumed equal to unity. They further assumed the approaching flow Froude number is equal to the flow intensity at incipient motion conditions and both are equal to unity. The maximum scour depth, d_{se} was determined using the following relationship:

$$\frac{d_{se}}{L} = 0.51 \left(\frac{y}{L}\right)^{0.5} \left(\frac{L}{B}\right)^{-0.5} (1 - R)^2 \quad (1)$$

where y is depth of flow, L is length of spur dike, B is width of main channel and R is the opening ratio. A considerable reduction in maximum scour depth was observed. It is worth mentioning that Equation (1) is independent of the approaching flow Froude number by assuming that the experiments were conducted under incipient motion conditions and that flow intensity is equal to Froude number. This assumption may not be true because critical flow conditions does not necessarily mean incipient motion conditions. Kang *et al.* (2011) experimentally investigated the flow characteristics for permeable spur dikes of different opening ratios. They observed a decrease in the velocity, the vortex strength, and the scale of the recirculation zone at the tip of the permeable spur dike as the opening ratio increases. Its resistance to the flow is lower than that of the permeable spur dike. By varying the opening ratio, the flow gradient along the bank can be adjusted. However, to maintain a navigation channel, this type of spur dike is less suitable. Zhang *et al.* (2013) investigated the bed variation around a hybrid type of spur dikes which is a combination of both impermeable and permeable dikes.

In the present study, the maximum scour depth occurring at permeable and impermeable spur dikes is simulated using the iRIC 2DH numerical model and the results are experimentally verified. Also, a nonlinear regression model is developed to predict the relative maximum scour depth using the experimental data. Both simulated and predicted results were tested for their accuracy and compared to that previously developed by Nasrollahi *et al.* (2008).

EXPERIMENTAL ARRANGEMENT

The experiments were carried out in the horizontal floor flume shown in Figure 1. The flume is 10 m long, 0.74 m wide, and 0.6 m high. The bed material with a thickness of 0.15 m is composed of non-cohesive uniform sand of $d_{50} = 0.75$ mm size. All experiments were conducted under

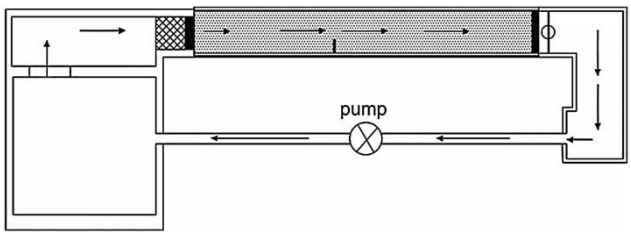

Figure 1 | Experimental floor flume.

clear water condition where the flow intensity V/Vc is less than unity. As shown in Figure 2, five constant length spur dike models having different permeability ratios, P_r, of 0, 0.23, 0.35, 0.45, and 0.55 were used, where $P_r = 0$ represents the case of impermeable spur dike (reference case). It has to be noted that P_r is defined as:

$$P_r = \frac{n.x}{L} \tag{2}$$

where L is length of spur dike, n is number of openings, and x is width of opening.

All spur dike models were made of polished wood of thickness 3 cm and 15 cm length which provides a contraction ratio of 0.2 which was kept constant for all dike models. The spur dikes were placed at right angles with the flow direction. A discharge of 0.02 m^3/s was kept constant for each of the five spur dike models with different water depths of 0.12, 0.1, and 0.08 m adjusted by the pivoted tailgate located at the downstream end of the channel and which provided different values of Froude number, Fr, ranging from 0.2 to 0.37. The discharge was measured using a calibrated sharp crested rectangular weir located at the entrance of the intake sump. After equilibrium scour condition was reached, scour depths were measured using digital point gauge with an accuracy of ±0.1 mm. Figure 3

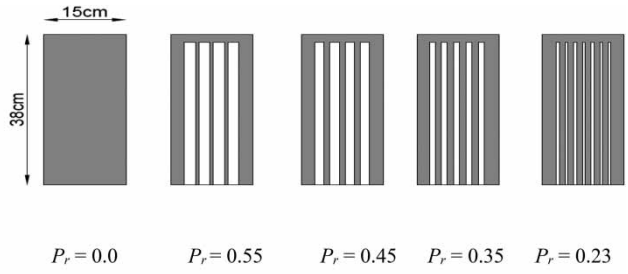

Figure 2 | Spur dike models of different opening ratios.

Figure 3 | Scour views for impermeable and permeable spur dikes.

shows views of the scour pattern at equilibrium stage for both permeable and impermeable spur dikes.

It has previously been reported that 94% of the scour process almost occurs within the first 3 hours (Masjedi *et al.* 2010). Karami *et al.* (2012) concluded that 70–90% of the scour process occurs within the first 20% of the equilibrium time. Therefore, the time to equilibrium in the present study was considered to be approximately 3 hours.

NUMERICAL MODEL

Many computational fluid dynamics (CFD) models, namely, SSIIM 2.0, Fluent and flow 3-D have been developed and applied by several researchers for simulating flow and scour around spur dikes. In the present study, the Nays-2DH model of the iRIC software package (Shimizu & Takebayashi 2011), which is available at http://www.i-ric.org is presented to test its capability in simulating flow and sediment transport around spur dikes. The model has previously been used by Allauddin & Tsujimoto (2012), Kaffle (2014), and Shahjahan *et al.* (2017). The results of the numerical model obtained in the present study are verified using the experimental data collected in this study.

The basic two-dimensional hydrodynamic equations in an orthogonal coordinate system (x, y) for the model are given as follows (Nays-2DH solver manual).

Continuity equation:

$$\frac{\partial h}{\partial t} + \frac{\partial (hu)}{\partial x} + \frac{\partial (hv)}{\partial y} = 0 \tag{3}$$

Momentum equations in x- and y-directions:

$$\frac{\partial(uh)}{\partial t}+\frac{\partial(hu^2)}{\partial x}+\frac{\partial(huv)}{\partial y}=-gh\frac{\partial H}{\partial x}-\frac{\tau_x}{\rho}+D^x \quad (4)$$

$$\frac{\partial(vh)}{\partial t}+\frac{\partial(huv)}{\partial x}+\frac{\partial(hv^2)}{\partial y}=-gh\frac{\partial H}{\partial y}-\frac{\tau_y}{\rho}+D^y \quad (5)$$

in which

$$\frac{\tau_x}{\rho}=C_f\,u\,\sqrt{u^2+v^2}\quad \frac{\tau_x}{\rho}=C_f\,v\,\sqrt{u^2+v^2}$$

$$D^x=\frac{\partial}{\partial x}\left[v_t h\frac{\partial u}{\partial x}\right]+\frac{\partial}{\partial y}\left[v_t h\frac{\partial u}{\partial y}\right]$$

$$D^y=\frac{\partial}{\partial x}\left[v_t h\frac{\partial v}{\partial x}\right]+\frac{\partial}{\partial y}\left[v_t h\frac{\partial v}{\partial y}\right]$$

$$C_f=\frac{gn_m^2}{h^{1/3}}$$

$$n_m=\frac{K_s^{1/6}}{7.66\sqrt{g}}$$

where h is water depth at time t, u and v are depth-averaged velocities in x- and y-directions, g is gravitational acceleration, H is the total water depth, τ_x and τ_y are the components of the shear stress of river bed in x and y directions, C_f is the drag coefficient of the bed shear stress, ν_t is eddy viscosity coefficient, and n_m is the Manning's coefficient of roughness. The depth-averaged k-ε model is used as turbulence model with finite differential advections as upwind scheme.

Sediment transport equations

The two-dimensional sediment continuity equation for bed load is expressed as:

$$\frac{\partial z_b}{\partial t}+\frac{1}{(1-\lambda)}\left(\frac{\partial q_{bx}}{\partial x}+\frac{\partial q_{by}}{\partial y}\right) \quad (6)$$

where z_b is the bed elevation, q_{bx} and q_{by} are the bed load transport in x- and y-directions, and λ is the porosity of the bed material. The model allows the user to calculate both q_{bx} and q_{by} using either Ashida & Michiue (1972) or Meyer-Peter & Muller (1948) formulae. In the present study, the Meyer-Peter and Müller bed load formula was used, which is given by:

$$q_b=8(\tau*-\tau_{*c})^{1.5}\cdot\sqrt{S_g\,g\,d^3}.r_b \quad (7)$$

where $\tau*$ is non-dimensional bed shear stress, τ_{*c} is critical shear stress, r_b is hydraulic radius of bed and S_g is grain specific weight.

GRID GENERATION AND COMPUTATIONAL SCHEME

A constant computational domain of 1.0 m in the x-direction with a total number of 41 grid points and 0.74 m in the y-direction with a number of grid points that varies according to the width of the opening such that each opening is represented by two cells as illustrated in Figure 4, which shows that for the case of opening width of 0.017 m corresponding to an opening ratio, Pr, of 0.45, a total number of 88 grid points was considered. The governing equations for velocities and shear stresses were discretized by finite difference method and then solved for the unknown values by an iterative procedure at each grid point in the computational domain with the boundary conditions set by considering a constant discharge of 0.02 m^3/sec at the upstream end and a constant depth of 0.12, 0.1, and 0.08 m at the downstream end. The sediment transport model was then solved using the bed load formula and used to compute the change in bed elevations using the sediment continuity equation.

EXPERIMENTAL RESULTS, ANALYSIS, AND DISCUSSION

Figure 5 shows the decrease of the relative maximum scour depth with the increase of the opening ratio. The figure also illustrates the increase of the relative scour depth with the increase of the Froude number. A remarkable reduction in the scour depth is observed for permeable spur dikes than impermeable ones especially at higher values of Froude number. For values of opening ratio of 0.23, the reduction reaches about 30% and reaches 80% for opening ratio of 0.55.

Figures 6 and 7 show the scour depth contours and bed topography for both permeable and impermeable spur dikes, respectively.

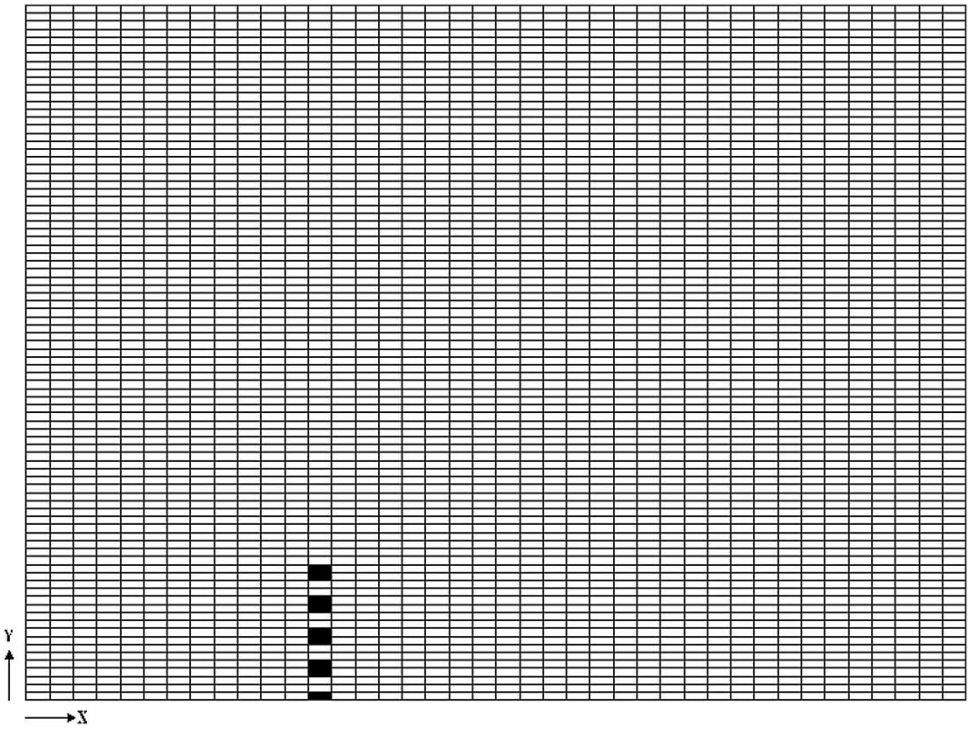

Figure 4 | Input of 41 × 88 grid for simulation, $y = 0.1$ m and $P_r = 0.45$.

Based on the experimental data collected in the present study, an empirical equation is obtained using nonlinear regression to determine the relative maximum scour depth as a function of both Froude number and opening ratio in the form:

$$\frac{d_s}{y} = 10.743\, F_r^{1.941}\, (1 - P_r)^{1.374} \tag{8}$$

Figure 8 shows the line of perfect agreement between the predicted relative scour depth using Equation (8) and the observed data at equilibrium stage with R^2 of 0.968 and RMSE of 0.066. This means that the regression model predicted the relative scour depth as a function of Froude number and opening ratio with the highest possible degree of accuracy for the range of data presented in this study.

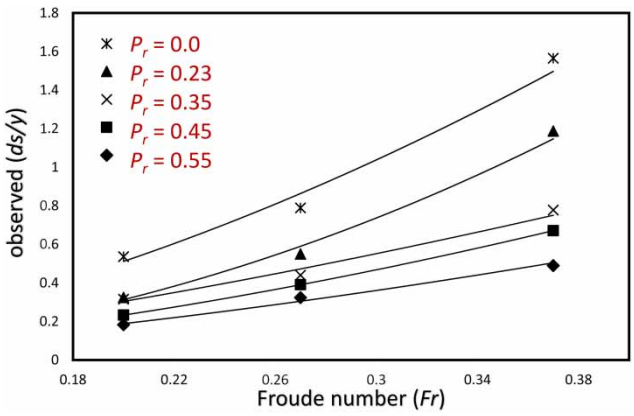

Figure 5 | Variation of (*ds/y*) with Froude number for different opening ratios.

NUMERICAL RESULTS AND ANALYSIS

Figure 9 illustrates the change in flow pattern (streamlines and velocity vectors) as obtained from the results of the numerical model for both impermeable and permeable spur dikes. The penetration of flow through the dike openings for permeable dikes and the deviation of the flow away from the banks for impermeable dikes are clearly detected by the model.

Figure 10 illustrates the accuracy of the numerical model to simulate the relative scour depth as compared to the observed data. An acceptable agreement is obtained as the statistical indices RMSE and R^2 were determined as 0.125 and 0.859, respectively. The numerical model is very sensitive to the value of Manning's n_m calculated as a function of the average roughness height k_s for the given d_{50} of the bed material (Kafle 2014).

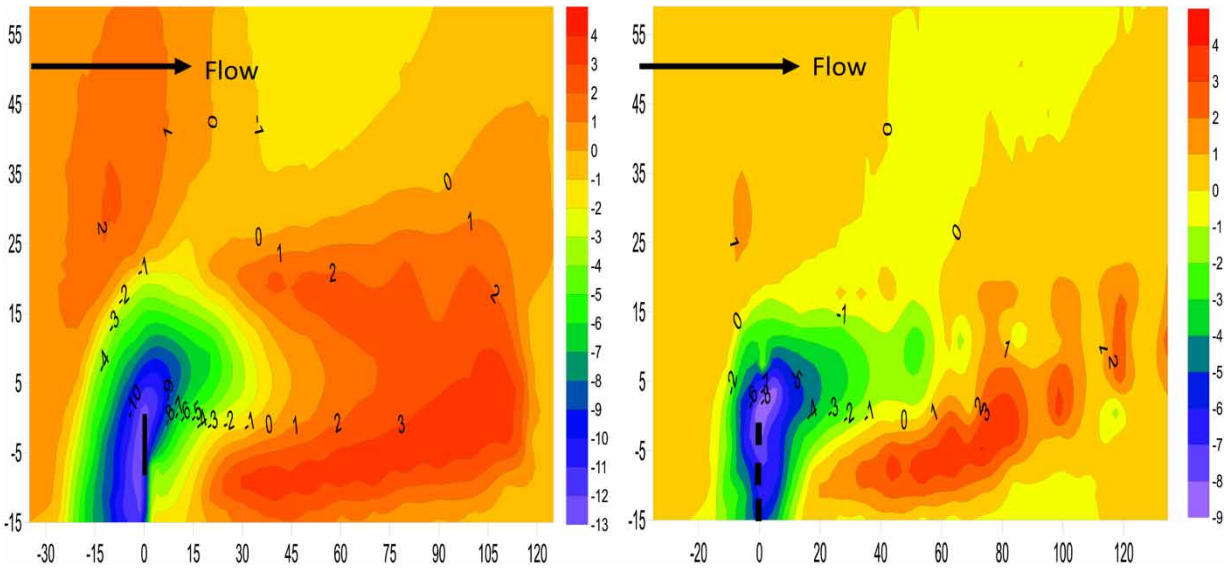

Figure 6 | Scour depth contours.

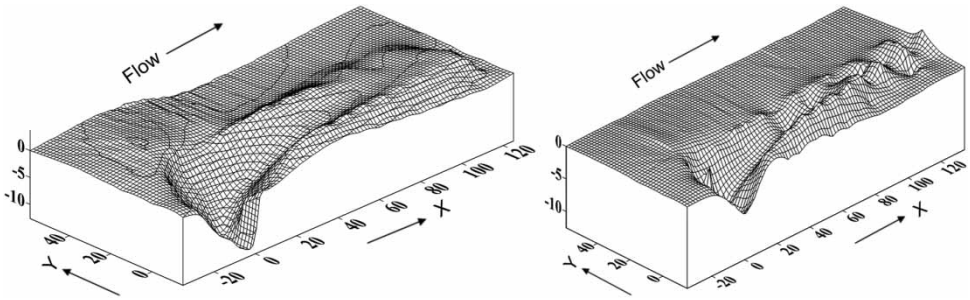

Figure 7 | Bed scour topography.

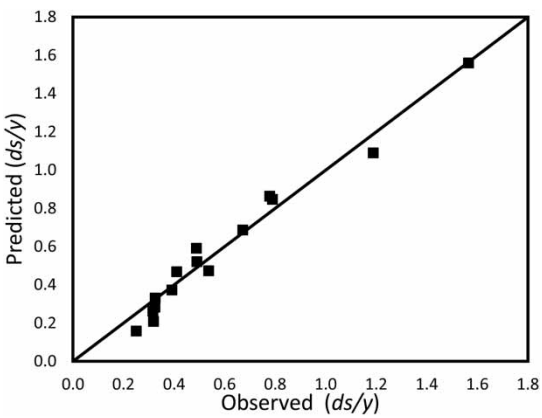

Figure 8 | Agreement between predicted (*ds/y*) using Equation (8) and observed data.

The values of (*ds/y*) determined using Equation (1) by Nasrollahi *et al.* (2008) are tested against the observed values and the results led to a fairly poor agreement. The scatter shown in Figure 11 and the values of the statistical indices RMSE and R^2 of 0.409 and 0.312, respectively, led to the key role of Froude number as an input variable in determining the scour depth for both permeable and impermeable spur dikes.

A summary of the values of the statistical indices RMSE and R^2 is shown in Table 1, and which indicates that the non-linear regression model presented by Equation (7) better predicted the relative maximum scour depth (*ds/y*) than both numerical model and Nasrollahi *et al.* (2008) regression model.

CONCLUSION

Permeable spur dikes as river training structures are very effective in reducing the scour depth produced by impermeable spur dikes. Extensive research work has been

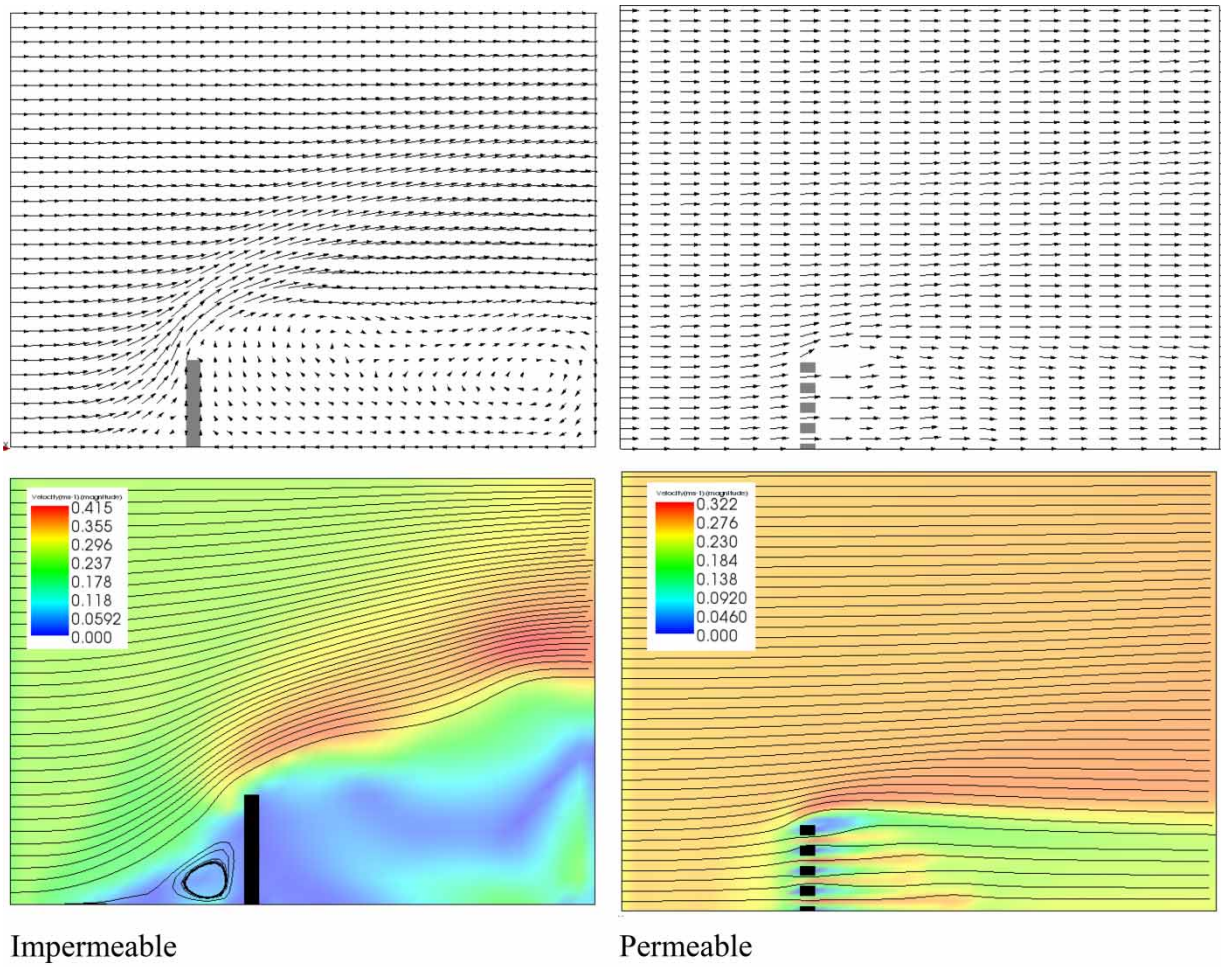

Figure 9 | Changes in flow pattern (streamlines and velocity vectors) due to permeability effect for $P_r = 0.23$ and water depth 0.1 m.

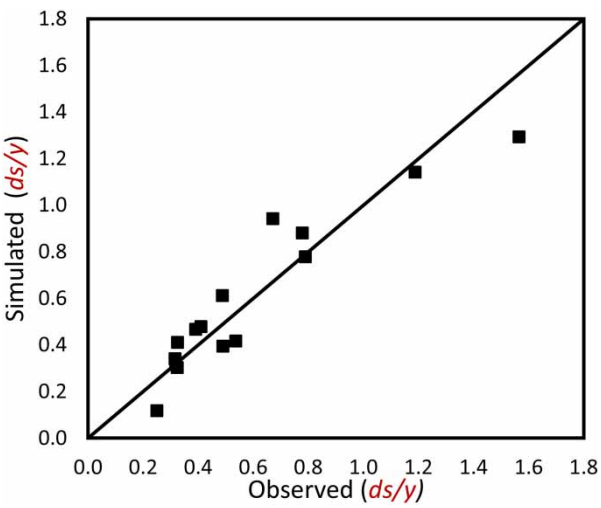

Figure 10 | Agreement between simulated (*ds/y*) and observed data.

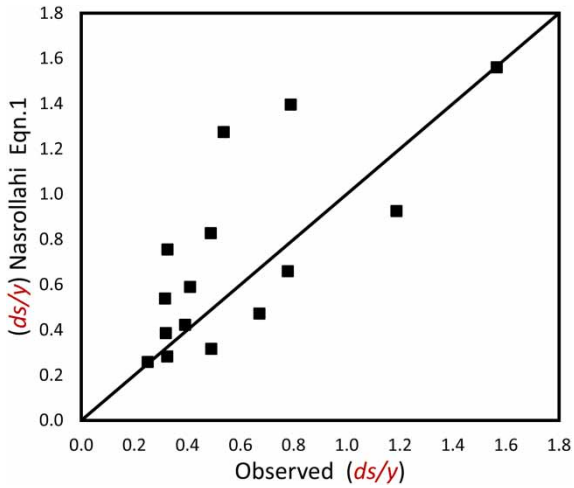

Figure 11 | Comparison between (*ds/dy*) by Nasrollahi *et al.* (2008) Equation (1), and observed data.

Table 1 | Values of the statistical indices for the relative scour depth (ds/y)

Statistical index Relative scour depth (d_s/y)	RMSE	R^2
Predicted (nonlinear regression), Equation (8)	0.066	0.968
Simulated (Nays-2DH)	0.125	0.859
Nasrollahi *et al.* (2008), Equation (1)	0.409	0.312

conducted for the determination of the maximum scour depth for impermeable spur dikes. However, very few equations are available for the determination of the maximum scour depth for permeable spur dikes. In this research, the relative maximum scour depth was numerically and experimentally investigated for permeable spur dikes with different opening ratios under different flow conditions.

A new empirical equation was developed using the experimental data and showed a better accuracy than the numerical results. The Nays-2DH numerical model of the iRIC software package simulated the scour around permeable and impermeable spur dikes with an acceptable degree of accuracy when verified by the experimental data, and although it is a 2D model, proved to be a promising numerical model for simulating bed and bank erosion in open channels. Furthermore, the accuracy of the numerical model is very sensitive to the estimation of the Manning's roughness coefficient for the given bed material. It was found that the maximum scour depth for permeable spur dikes is a function of both approaching flow Froude number and opening ratio. The reduction in scour depth for permeable spur dikes could reach up to 68% of its respective value for impermeable spur dikes for an opening ratio of 55%. The empirical equation developed by Nasrollahi *et al.* (2008) which is independent of the approaching flow Froude number showed poor agreement when validated through the experimental data, which means that the Froude number is the key role in determining the scour depth for both permeable and impermeable spur dikes.

REFERENCES

Allauddin, M. & Tsujimoto, M. 2012 Optimal configuration of groynes for stabilization of alluvial rivers with fine sediments. *International Journal of Sediment Research* **27** (2), 158–167.

Ashida, K. & Michiue, M. 1972 Studies on Bed Load Transportation for Nonuniform Sediment and River Bed Variation. Disaster Prevention Research Institute Annuals, Kyoto University, No. 14B, pp. 259–273.

Ettema, R. & Muste, M. 2004 Scale effects in flume experiments on flow around a spur dike in flat bed channel. *ASCE Journal of Hydraulic Engineering* **130** (7), 635.

Fukuoka, S., Watanabe, A., Kawaguchi, H. & Yasutake, Y. 2000 A study of permeable groins in series installed in a straight channel. *Proceedings of Hydraulic Engineering* **44**, 1047–1052.

Gu, Z. P., Akahori, R. & Ikeda, S. 2011 Study on the transport of suspended sediment in an open channel flow with permeable spur dikes. *International Journal of Sediment Research* **26** (1), 96–111.

Kafle, M. 2014 Numerical simulation of flow around a spur dike with free surface flow in fixed flat bed. *Journal of the Institute of Engineering* **9** (1), 107–114.

Kang, J., Yeo, H., Kim, S. & Ji, U. 2011 Permeability effects of single groyne on flow characteristics. *Journal of Hydraulic Research* **49** (6), 1–8.

Karami, H., Ardeshir, A., Saneie, M. & Salamatin, A. 2012 Prediction of time variation of scour around spur dikes using neural network. *Journal of Hydroinformatics* **14** (1), 180–191.

Li, Z. S., Michioku, K., Maeno, S., Ushita, T. & Fujii, A. 2005 Hydraulic characteristics of a group of permeable groins constructed in an open channel flow. *Journal of Applied Mechanics* **8**, 773–782.

Masjedi, A., Nadri, A., Taeedi, A. & Masjedi, I. 2010 Control of local scour at single L-dike with wing shape in flume bed. *Journal of American Science* **6** (10), 893–897.

Meyer-Peter, E. & Muller, R. 1948 Formulas for Bed Load Transport IAHR Report on the Second Meeting **3**, pp. 39–64.

Nasrollahi, A., Ghodsian, M. & Neyshabouri, S. 2008 Local scour at permeable spur dikes. *Journal of Applied Sciences Asian Network for Scientific Information* **8** (19), 3398–3406.

Pandy, M., Ahmad, Z. & Sharma, P. K. 2015 Estimation of maximum scour depth near a spur dike. *Canadian Journal of Civil Engineering* **43** (3), 270–278.

Shahjahan, M., Hasan, M. & Haque, M. 2017 Simulation of flow in an open channel with groin-like structures by iRIC Nays2DH. *Mathematical Problems in Engineering* **2017**, 1–10.

Shimizu, Y. & Takebayashi, H. 2011 *Nays 2DH Solver Manual*. iRIC Software.

Zhang, H., Nakagawa, H., Ogura, M. & Mizutani, H. 2013 Experiment study on channel bed characteristics around spur dikes of different shape. *Journal of Applied Mechanics* **69** (2), 489–499.

First received 14 October 2018; accepted in revised form 10 January 2019. Available online 1 February 2019